Origin of the high-energy kink in the photoemission spectrum of the high-temperature superconductor $Bi_2Sr_2CaCu_2O_8$

Susmita Basak,[1] Tanmoy Das,[1] Hsin Lin,[1] J. Nieminen,[1,2] M. Lindroos,[1,2] R. S. Markiewicz,[1,3,4] and A. Bansil[1]
[1]*Physics Department, Northeastern University, Boston, Massachusetts 02115, USA*
[2]*Institute of Physics, Tampere University of Technology, P.O. Box 692, 33101 Tampere, Finland*
[3]*SMC-INFM-CNR, Dipartimento di Fisica, Università di Roma "La Sapienza," P. Aldo Moro 2, 00185 Roma, Italy*
[4]*ISC-CNR, Via dei Taurini 19, 00185 Roma, Italy*
(Received 16 November 2009; published 17 December 2009)

The high-energy kink or the waterfall effect seen in the photoemission spectra of cuprates is suggestive of the coupling of quasiparticles to a high-energy bosonic mode with implications for the mechanism of superconductivity. Recent experiments, however, indicate that this effect may be an artifact produced entirely by matrix element effects, i.e., by the way the photoemitted electron couples to incident photons in the emission process. In order to address this issue directly, we have carried out realistic computations of the photointensity in $Bi_2Sr_2CaCu_2O_8$ where the effects of the matrix element are included together with those of the corrections to the self-energy resulting from electronic excitations. Our results demonstrate that while the photoemission matrix element plays an important role in shaping the spectra, the waterfall effect is a clear signature of the presence of strong coupling of quasiparticles to electronic excitations.

DOI: 10.1103/PhysRevB.80.214520 PACS number(s): 79.60.−i, 74.20.Mn, 74.25.Jb, 74.72.Hs

I. INTRODUCTION

An anomalous "high-energy kink" (HEK) in dispersion, which gives the associated angle-resolved photoemission (ARPES) spectrum the appearance of a "waterfall" was first seen[1,2] in $Bi_2Sr_2CaCu_2O_8$ (Bi2212) cuprate superconductors. Such HEKs or waterfalls have now been established as being a universal feature in the cuprates,[1–3] and interpreted as providing evidence for interaction of the quasiparticles with some bosonic mode of the system.[4,5] The high-energy scale of this boson (~500 meV) would then provide a tangible electronic mechanism of high-temperature superconductivity.[6,7] However, recent experiments show that the HEK is quite sensitive to matrix element (ME) effects, i.e., to the nature of the photoemission process itself, or in other words, the way the incident photon couples with the electronic states of the system in generating the photoemitted electrons. In particular, the ARPES spectra undergo substantial changes in shape as one probes the electronic states by varying the energy of the incident photon or the momentum of the outgoing electron.[8–10] In Bi2212, for example, the shape of the ARPES spectrum varies with photon energy from a shape that displays a single band tail with relatively large intensity giving the spectrum a "Y" shape, to a spectrum which shows the presence of double tails with a waterfall.[11] These results have led to speculation that the HEK may be an artifact produced entirely by ME effects, questioning thus the fundamental importance of the waterfall effect in the physics of correlated electron systems.[8,11,12]

In order to address this controversy, we have carried out first-principles, one-step photointensity computations in Bi2212 in which we include not only the effects of the ARPES matrix element but also incorporate a model self-energy based on accurate susceptibility calculations which properly reproduce the HEK phenomenology.[4,13–18] In this way, we establish conclusively that despite a strong modulation of the spectra due to the ARPES matrix element, a genuine HEK or a waterfall effect is still present in the cuprates, and that its presence indicates a significant coupling to bosons of electronic origin. Given the strength of the coupling and the associated high-energy scale, these bosons will play an important role in the Mott as well as the superconducting physics of the cuprates. In this connection, we also discuss model ARPES computations based on a simplified tight-binding model for the purpose of gaining a handle on the interplay between the matrix element and self-energy effects, and for delineating the nature of the striking characteristics of the ARPES matrix element such as the crossover from the Y-type spectral shape to the waterfall shape with photon energy. In this study, we consider the overdoped normal state where the pseudogap and superconducting gap are absent, allowing us to highlight the waterfall effect. In any event, the waterfall physics is insensitive to the presence of the low-energy pseudogap or the superconducting gap.[17,19]

II. "WATERFALL" PHENOMENON IN FIRST-PRINCIPLES CALCULATIONS

We discuss our key findings with reference to Fig. 1. Note first how the shape of the experimental spectrum changes dramatically at different photon energies. In panel (a) at 81 eV, the spectral intensity presents the appearance of a pair of waterfalls with a region of low intensity through the middle of the figure. This is in sharp contrast to the measured spectrum in (b) at 64 eV where we see a "Y shape" with the two arms of the Y connecting a vertical region of high intensity. Our realistic first-principles photointensity computations in which the matrix element as well as self-energy effects are accounted for reproduce the characteristic features of these shapes, the waterfall shape in panel (c) at 81 eV and the Y shape in panel (d) at 64 eV. In panels (e) and (f) we have *excluded* the self-energy corrections in the photointensity computations. It is seen immediately that the results of panels (e) and (f) bear little resemblance to the experimental

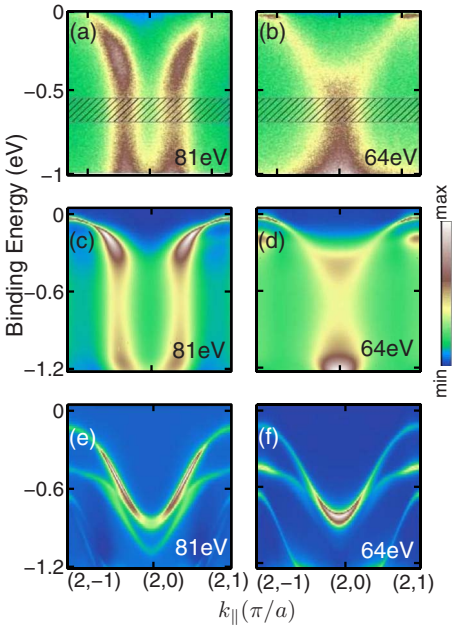

FIG. 1. (Color online) ARPES spectra in Bi2212. (a) and (b) are experimental results at photon energies of 81 and 64 eV, respectively (Ref. 11). (c) and (d) are the corresponding theoretical photoemission spectra based on first-principles one-step calculations in which the self-energy correction is *included*. (e) and (f) computations where the self-energy correction is *excluded* to highlight the key role of self-energy corrections in explaining the experimentally observed waterfall effect (Ref. 20).

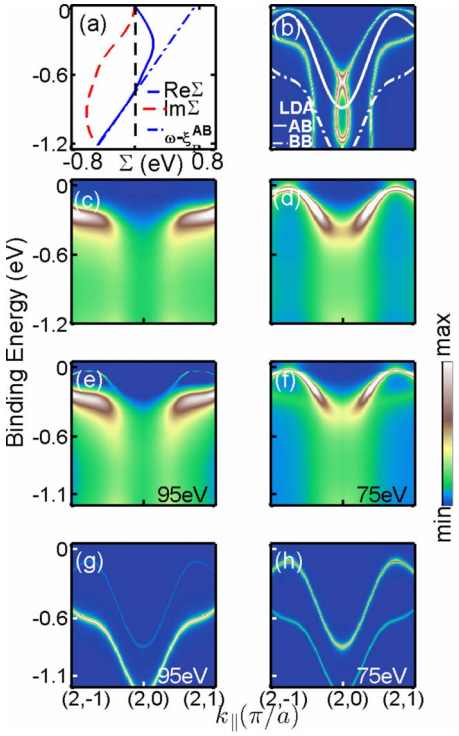

FIG. 2. (Color online) Model self-energy and spectral weight in Bi2212. (a) Real (blue solid line) and imaginary (red dashed line) parts of the computed self-energy used in photointensity computations. The blue dash-dotted line gives $\omega-\xi_{\Gamma}^{AB}$. (b) Dispersion renormalized by the real part of the self-energy in (a) is compared to the bare dispersion of the antibonding band (AB, white solid line) and the bonding band (BB, white dash-dotted line). (c) and (d) spectral weights dressed by real and imaginary parts of the self-energy for AB and BB, respectively. (e) and (f) photoemission intensities obtained after incorporating the matrix elements at the two indicated photon energies. (g) and (h) are photoemission intensities with matrix element effects, but without including the self-energy correction.

spectra even though these computations include the effects of the ARPES matrix element.[20] The comparisons of Fig. 1 show very clearly that the waterfall effect cannot be obtained through the effect of the ARPES matrix element alone. We emphasize that we obtain our many-body self-energy correction self-consistently by computing the susceptibility within a GW-type scheme, which is applicable to the entire doping range to model not only the waterfall physics but also the pseudogap and the superconducting gap; see Sec. V and Appendix A for details of the self-energy computation. As already noted, here we focus on the overdoped case to highlight the waterfall effect.

III. UNDERSTANDING THE SEPARATE ROLES OF SELF-ENERGY AND MATRIX ELEMENT IN THE "WATERFALL" FEATURE

For the purpose of delineating the roles of the self-energy and matrix elements in shaping the ARPES spectra, Fig. 2 presents the results of photointensity computations based on a simplified two-band tight-binding Hamiltonian which models the low-energy electronic structure of Bi2212.[21,22] We have used a tight-binding fit to the local-density approximation (LDA) dispersion[23–27] and the same self-energy as in the first-principles calculation of Fig. 1 above, whose real and imaginary parts are shown in Fig. 2(a) for the antibonding band (AB) [similar results for the bonding band (BB) are not shown for brevity]. The model bands dressed by only the real part of the self-energy are shown in Fig. 2(b), together with the LDA bands at $k_z=2\pi/c$ (magenta lines). The real part of the self-energy [solid blue line in (a)] is almost linear in ω in the low-energy region. We write the slope of the linear part as $(1-Z^{-1})$ to define the renormalization coefficient Z. This leads to a renormalized quasiparticle dispersion $\bar{\xi}_{\mathbf{k}}=Z\xi_{\mathbf{k}}$, which, e.g., reduces the bilayer splitting between the AB and BB at the antinodal point to $Z(\xi_{\pi,0}^{AB}-\xi_{\pi,0}^{BB})$, consistent with experimental results.[8,22] In contrast, at the Γ point the self-energy $\Sigma'(\xi_{\Gamma}^{AB/BB})$ is negative,[28] so that the dressed bands determined by $\xi_{\Gamma}^{AB/BB}+\Sigma'(\xi_{\Gamma}^{AB/BB})$ move further away from each other.[29] These opposing tendencies at low and high energies, which are seen clearly in the experimental spectra,[30] are an unambiguous signature of strong coupling to a bosonic mode at intermediate energy.

When the imaginary part of the self-energy Σ'' is turned on, interesting spectral weight modulations emerge, which are shown separately in Figs. 2(c) and 2(d) for the AB and BB, respectively. Σ'' plays a crucial role in redistributing spectral weight such that the weight is shifted from the coherent region near the Fermi energy into incoherent parts at higher energies to produce the HEK features seen

experimentally.[4] However, the differences noted earlier near Γ lead to striking differences in the manifestation of the kink effect in the AB and BB spectra. In AB, the band bottom at Γ lies above the waterfall region, and Σ″ creates a long tail in the dispersion extending to high energies,[31] so that the fully dressed band exhibits the Y-shaped pattern of panel (c). In contrast, the waterfall shape emerges distinctly in the bonding band in panel (d) where the band bottom lies below the boson peak. These two dispersions are remarkably close to the two experimental dispersions observed at different photon energies as seen in Figs. 1(a) and 1(b) (Ref. 11) and provide insight into the nature of the waterfall phenomenon in the spectra. Figures 2(e) and 2(f) show how when the photointensity is computed for the bilayer system, the matrix element highlights the AB or BB at two different photon energies in accord with the experimental spectra. In sharp contrast, when the self-energy correction is removed from the computations in Figs. 2(g) and 2(h), the waterfall effect disappears, even in the presence of matrix element effects, leaving only the underlying LDA dispersion.

IV. MODULATION OF "WATERFALL" SHAPE AND "Y" SHAPE AS A FUNCTION OF PHOTON ENERGY AND THE ROLE OF BILAYER SPLITTING

Insight into the energy dependence of the spectra and contributions of different orbitals therein can be obtained within the tight-binding framework. Details of our tight-binding photointensity computations are given in Appendix B. In particular, the tight-binding matrix element M can be written in terms of a structure factor $S_i^{\mu}(\mathbf{k}_f)$

$$M_{\mu}(\mathbf{k}_f) = \sum_i S_i^{\mu}(\mathbf{k}_f) e^{-i\mathbf{k}_f \cdot \mathbf{R}_i}. \tag{1}$$

Here μ is a band index, k_f is the momentum of the ejected electron. and $\mathbf{R_i}$ is the position of the ith atom in the unit cell.

For a bilayer system, the structure factor of Eq. (1) is independent of $k_f^{\perp}$, and the matrix elements for the bilayer can be simply related to the matrix element of a single layer $M_{\mu}^{0}(\mathbf{k}_f^{\parallel})$

$$M_{\mu}^{\pm}(\mathbf{k}_f) = M_{\mu}^{0}(\mathbf{k}_f^{\parallel})[1 \pm e^{-ik_f^{\perp} d}], \tag{2}$$

where the + sign refers to the AB and the − sign to the BB, and d denotes the separation of the CuO_2 layers in a bilayer.[32,33] The key feature of Eq. (2) is the interference term in brackets, where $k_f^{\perp}$ depends on the photon energy through[11,34]

$$k_f^{\perp} = \sqrt{\frac{2m}{\hbar^2}(h\nu - E_{bind} - \Phi + V_0) - (k_{\parallel} + n_{\parallel} G_{\parallel})^2}, \tag{3}$$

where $h\nu$ is the incident photon energy and $E_{bind} \approx 0.6$ eV is the binding energy of the electron in the solid at the waterfall, $\Phi \approx 4$ eV is the work function, $V_0 = 10$ eV is the inner potential of the crystal and $k_{\parallel} + n_{\parallel} G_{\parallel}$ is the total in-plane wave number, which we have taken to be $\approx 2\pi/a$ to match the experimental conditions.[35] Since the two bilayer terms in Eq. (2) are out of phase (note ± sign)], whenever $k_f^{\perp} d$ changes by π, the spectrum would switch from the odd to the even bilayer, a change that can be induced in view of Eq. (3) via the photon frequency ν. This behavior is indeed seen in panels (e) and (f) of Fig. 2 where the matrix element is incorporated in the photointensity computations using Eqs. (1)–(3). In particular, at 75 eV in panel (f), the AB gets highlighted resulting in a Y-shaped spectrum with a tail extending to high energies. In contrast, in panel (e) at 95 eV, the bonding band dominates and spectral shape reverts to that of a waterfall with a double tail.

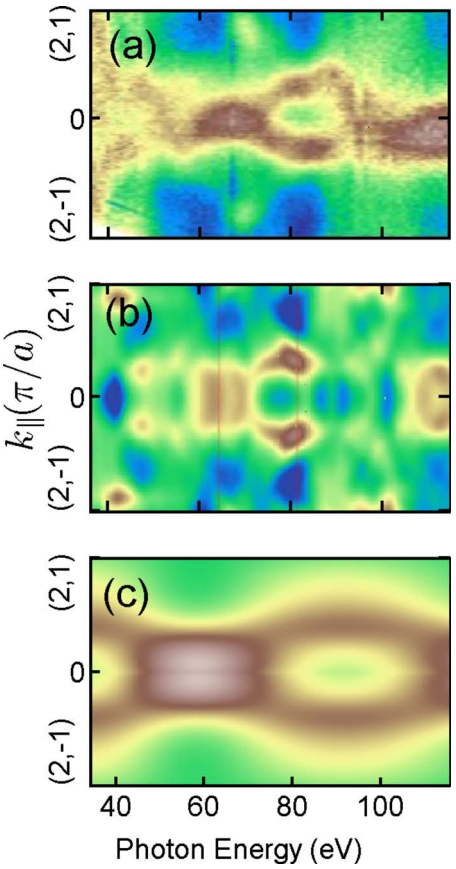

FIG. 3. (Color online) Spectral weight integrated over the shaded binding-energy window of Fig. 1(a) and 1(b) in the intermediate energy region is shown to highlight how the spectra vary between the Y and waterfall shapes as a function of photon energy. (a) Experimental spectral weights normalized to the peak intensity at each energy (Ref. 11). (b) Theoretical weights corresponding to the first-principles computations of spectra in Figs. 1(c) and 1(d). (c) Corresponding weights based on the tight-binding spectra of Figs. 2(e) and 2(f). Color scheme is the same as in Fig. 1.

Along the preceding lines, Fig. 3 further discusses the Y to waterfall shape change as a function of the photon energy. For this purpose, we consider in Fig. 3 the integrated spectral weight over the shaded binding-energy window shown in Fig. 1(a) and 1(b). The Y shape is then characterized by a relatively narrow single tail in momentum (vertical axis in Fig. 3), while the waterfall displays a splitting of this feature due to the presence of two tails. The experimental results of Ref. 11 shown in Fig. 3(a) are seen to be in good accord with the corresponding first-principles computations in Fig. 3(b) and with tight-binding computations in Fig. 3(c), some dif-

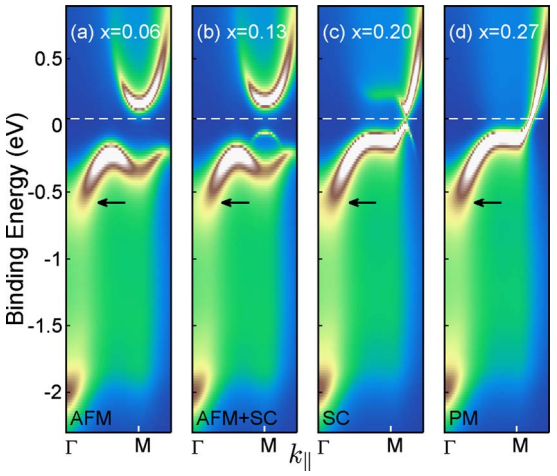

FIG. 4. (Color online) Spectral weight dressed by self-energy as a function of doping x as discussed in the text. Black arrows mark the onset of the waterfall feature.

ferences between theory and experiment with respect to the onset of Y or waterfall shape in photon energy notwithstanding.

V. DOPING DEPENDENCE OF "WATERFALL" PHENOMENON IN THE PRESENCE OF PSEUDOGAP AND SUPERCONDUCTING GAP

In order to explicate the role of matrix elements, we have focused on the relatively simpler overdoped case in the preceding sections. However, the present QP-GW scheme is applicable to the entire doping range from the half-filled to the overdoped state and it thus models the pseudogap and superconducting (SC) physics including the waterfall features.

The pseudogap is modeled here as due to (π,π) antiferromagnetic order and the d-wave superconductivity is treated within the BCS theory where the pairing potential is fitted to the experimental gap value. We illustrate the comprehensive nature of our self-energy in the Bi2212 system (here we focus on the antibonding band only) with reference to Fig. 4, which gives the evolution of the spectral weight in going from the insulating to the overdoped system. Note that the spectral weight in the low-energy region near the Fermi energy undergoes substantial changes as we go from the AFM insulator in panel (a) for doping $x=0.06$, to the [AFM+SC] case in panel (b), to the SC case only in panel (c), to finally the paramagnetic case of panel (d) for the overdoped system. The key point to note is that despite these large changes in the low-energy region, the waterfall region is virtually unaffected throughout the entire doping range with the waterfall feature starting at roughly the same energy (shown by arrow).

VI. CONCLUSION

In summary, we have carried out computations of the photointensity in Bi2212 where the effects of the photoemission matrix element as well those of the coupling of the quasiparticles to electronic excitations are included realistically.[36–40] We thus establish that despite the importance of the matrix element in shaping the spectra, the waterfall effect is a clear signature of the coupling of the electronic system to a high-energy bosonic mode, which bears on the physics of the pseudogap[17,41] and the mechanism of high-temperature superconductivity.[6,7] Our analysis of the spectra based on a simplified two-band tight-binding model reveals how the near-Fermi-energy bonding and antibonding bands associated with the CuO_2 bilayers in Bi2212 produce characteristic Y shape and waterfall shape of the spectrum as a function of the energy of the incident photons. Such a modulation of the spectrum with photon energy may provide a new spectroscopic tool for getting a handle on the structural aspects of the bilayer via the photoemission technique.

ACKNOWLEDGMENTS

We thank J. Lorenzana for discussions. This work is supported by the U.S. Department of Energy, Office of Science, Division of Materials Science and Engineering, under Grant No. DE-FG02-07ER46352, and benefited from the allocation of supercomputer time at NERSC, Northeastern University's Advanced Scientific Computation Center (ASCC), the Institute of Advanced Computing (IAC), Tampere, and Techila Technologies computational solutions. R.S.M.'s work has been partially funded by the Marie Curie Foundation under Grant No. PIIF-GA-2008-220790 SOQCS.

APPENDIX A: DETAILS OF SELF-ENERGY CALCULATION

Our starting point is a bilayer split tight-binding band where the dispersion is fitted to the first-principles LDA bands based on Cu $d_{x^2-y^2}$ and oxygen p_x and p_y orbitals. The self-energy is then computed by using the GW method as

$$\Sigma^{\nu}(\mathbf{k},i\omega_n)=\sum_{\nu'}\sum_{\mathbf{q}}\int_{-\infty}^{\infty}\frac{d\omega'}{2\pi}\Gamma G^{\nu'}(\mathbf{k}-\mathbf{q},i\omega_n+\omega')\times W^{\nu\nu'}(\mathbf{q},\omega'). \quad \text{(A1)}$$

Here G^{ν} is the single-particle Green's function for the antibonding ($\nu=+$) or the bonding ($\nu=-$) band and Γ is a vertex correction. The interaction term $W^{\nu\nu'}$ includes both spin and charge fluctuations and for the paramagnetic case can be written as $W^{\nu\nu'}=(U^2/2)\mathrm{Im}[3\chi_s^{\nu\nu'}+\chi_c^{\nu\nu'}]$. U is the onsite Hubbard U and $\chi_{s/c}^{\nu\nu'}$ is the spin/charge susceptibility due to intraband ($\nu=\nu'$) or interband ($\nu\neq\nu'$) correlations. Within the random-phase approximation,

$$\chi_{c/s}^{\nu\nu'}(\mathbf{q},\omega)=\sum_{\nu''}\chi_0^{\nu\nu''}(\mathbf{q},\omega)[1\pm U\chi_0(\mathbf{q},\omega)]^{-1}_{\nu''\nu'}, \quad \text{(A2)}$$

where the $\pm$ sign on the right-hand side of the equation refers to the charge/spin channel.

A variety of GW schemes have been presented in the literature and involve differences in the way the G and W terms on the right-hand side (rhs) of Eq. (A1) are approximated. In our particular scheme, which we refer to as the quasiparticle GW (QP-GW) scheme, the self-energy is evalu-

ated *self-consistently* using the low-energy expansion, $\Sigma_0'(\omega)=(1-Z^{-1})\omega$. The Green's function on the rhs of Eq. (A1) then becomes $G_Z^\nu=Zf(\bar{\xi}_{\mathbf{k}}^\nu)(i\omega_n-\bar{\xi}_{\mathbf{k}}^\nu)^{-1}$ with f being the Fermi function and $\bar{\xi}_{\mathbf{k}}^\nu=Z\xi_{\mathbf{k}}^\nu$, which leads to the bare two-particle correlation function,

$$\chi_{0Z}^{\nu\nu'}(\mathbf{q},i\omega_n)=\frac{1}{\beta}\sum_{\mathbf{k}}\sum_{n}G_Z^\nu(\mathbf{k},ip_n)G_Z^{\nu'}(\mathbf{k}+\mathbf{q},ip_n+i\omega_n)$$

$$=-Z^2\sum_{\mathbf{k}}\frac{f(\bar{\xi}_{\mathbf{k}}^\nu)-f(\bar{\xi}_{\mathbf{k}+\mathbf{q}}^{\nu'})}{i\omega_n+\bar{\xi}_{\mathbf{k}}^\nu-\bar{\xi}_{\mathbf{k}+\mathbf{q}}^{\nu'}} \tag{A3}$$

with $\beta=1/k_BT$. The vertex correction within Ward's identity is taken as $\Gamma_Z=1/Z$. Finally, the renormalization factor Z is found self-consistently by requiring that the input Σ_0-dressed dispersion and the final Σ-dressed dispersion agree in the low-energy region. Since the band parameters are taken from LDA, this means that the only free parameter in our GW scheme is the Hubbard U. In this study, doping is fixed in the optimal regime of Bi2212 with Hubbard $U=1$ eV, which is in accord with mean-field calculations.[4] We then obtain a self-consistent value of $Z=0.5$.

Although we have focused on the relatively simpler overdoped case above, where the pseudogap and the superconducting gap are not present in the spectrum, our QP-GW scheme and Eqs. (A1)–(A3) can be extended straightforwardly to model the self-energy over the entire doping range.

APPENDIX B: DETAILS OF PHOTOEMISSION MATRIX ELEMENT CALCULATION IN THE TIGHT-BINDING SCHEME

The matrix element for transition from an initial state $|\mu\rangle$ to the final state $|\mathbf{k_f}\rangle$ can be obtained using the standard Fermi's Golden rule for the μth band

$$M_\mu(\mathbf{k}_f)=\langle\mathbf{k_f}|\mathbf{A}\cdot\mathbf{p}|\mu\rangle$$

$$=\hbar A\hat{\epsilon}\cdot\mathbf{k}_f\sum_{j,nlm}(-i)^l Y_{lm}(\theta_{k_f},\phi_{k_f})F_{nl}(k_f)$$

$$\times\langle j,nlm|\mu\rangle e^{-i\mathbf{k}_f\cdot\mathbf{R}_j}. \tag{B1}$$

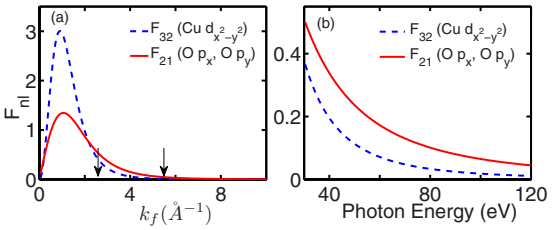

FIG. 5. (Color online) (a) Form factors of Eq. (B2) for copper $d_{x^2-y^2}$ orbital (dashed line), F_{32}, and for oxygen p orbital, F_{21}. Vertical arrows indicate the k_f range that corresponds to the final-state energies considered in Fig. 3. (b) Form factors are shown over the energy window marked by the arrows in (a). Note that here the k_f scale is converted into the energy scale.

Here $\mathbf{k}_f$ is the momentum of the ejected electron, $\hat{\epsilon}$ denotes the polarization of light with vector potential $\mathbf{A}$, and Y_{lm} is the spherical harmonic for the angular variables of $\mathbf{k}_f$. The final state is taken to be a free-electron state. The initial state $|\mu\rangle$ is a tight-binding state, which is expanded into atomic orbital (nlm) of the jth atom in the unit cell at position $\mathbf{R_j}$. The form factor

$$F_{nl}(k_f)=\int r^2 dr j_l(k_f r)R_{nl}(r), \tag{B2}$$

where j_l is a spherical Bessel function, is evaluated numerically using the radial part of the atomic wave function.

Figure 5(a) shows that at low k_f the Cu contribution F_{32} for the Cu $d_{x^2-y^2}$ orbital is dominant, while the oxygen contribution F_{21} for the oxygen p_x and p_y orbitals dominates for $k_f>2$ Å^{-1}. Although Eq. (B1) is general, in this study we have used only three orbitals, i.e., Cu $d_{x^2-y^2}$, O p_x, and O p_y in expanding the antibonding and bonding bands to obtain the photointensities for our illustrative purposes. Finally, Eq. (B1) can be recast into a useful form by collapsing all the symmetry information concerning the ith orbital into the structure factor $S_i^\mu(\mathbf{k}_f)$ as seen in Eq. (1) of the main text.

[1] F. Ronning, K. M. Shen, N. P. Armitage, A. Damascelli, D. H. Lu, Z. X. Shen, L. L. Miller, and C. Kim, Phys. Rev. B **71**, 094518 (2005).
[2] J. Graf, G.-H. Gweon, K. McElroy, S. Y. Zhou, C. Jozwiak, E. Rotenberg, A. Bill, T. Sasagawa, H. Eisaki, S. Uchida, H. Takagi, D.-H. Lee, and A. Lanzara, Phys. Rev. Lett. **98**, 067004 (2007).
[3] B. Moritz, F. Schmitt, W. Meevasana, S. Johnston, E. M. Motoyama, M. Greven, D. H. Lu, C. Kim, R. T. Scalettar, Z.-X. Shen, and T. P. Devereaux, New J. Phys. **11**, 093020 (2009).
[4] R. S. Markiewicz, S. Sahrakorpi, and A. Bansil, Phys. Rev. B **76**, 174514 (2007).
[5] A. Macridin, M. Jarrell, T. Maier, and D. J. Scalapino, Phys. Rev. Lett. **99**, 237001 (2007).
[6] T. Dahm, V. Hinkov, S. V. Borisenko, A. A. Kordyuk, V. B. Zabolotnyy, J. Fink, B. Büchner, D. J. Scalapino, W. Hanke, and B. Keimer, Nat. Phys. **5**, 217 (2009).
[7] R. S. Markiewicz and A. Bansil, Phys. Rev. B **78**, 134513 (2008).
[8] D. S. Inosov, J. Fink, A. A. Kordyuk, S. V. Borisenko, V. B. Zabolotnyy, R. Schuster, M. Knupfer, B. Büchner, R. Follath, H. A. Dürr, W. Eberhardt, V. Hinkov, B. Keimer, and H. Berger, Phys. Rev. Lett. **99**, 237002 (2007).
[9] W. Zhang, G. Liu, J. Meng, L. Zhao, H. Liu, X. Dong, W. Lu, J. S. Wen, Z. J. Xu, G. D. Gu, T. Sasagawa, G. Wang, Y. Zhu, H. Zhang, Y. Zhou, X. Wang, Z. Zhao, C. Chen, Z. Xu, and X. J. Zhou, Phys. Rev. Lett. **101**, 017002 (2008).
[10] Q. Wang, Z. Sun, E. Rotenberg, H. Berger, H. Eisaki, Y. Aiura,

and D. S. Dessau, arXiv:0910.2787v1 (unpublished).
[11] D. S. Inosov, R. Schuster, A. A. Kordyuk, J. Fink, S. V. Borisenko, V. B. Zabolotnyy, D. V. Evtushinsky, M. Knupfer, B. Büchner, R. Follath, and H. Berger, Phys. Rev. B **77**, 212504 (2008); **79**, 139901(E) (2009).
[12] For all polarizations and photon energies, the near-Fermi-surface features are strongly renormalized from LDA values, whereas the band bottom is not, which is normally considered a signature of a bosonic coupling.
[13] M. Lindroos, S. Sahrakorpi, and A. Bansil, Phys. Rev. B **65**, 054514 (2002).
[14] S. Sahrakorpi, M. Lindroos, R. S. Markiewicz, and A. Bansil, Phys. Rev. Lett. **95**, 157601 (2005).
[15] A. Bansil, M. Lindroos, S. Sahrakorpi, and R. S. Markiewicz, Phys. Rev. B **71**, 012503 (2005).
[16] M. C. Asensio, J. Avila, L. Roca, A. Tejeda, G. D. Gu, M. Lindroos, R. S. Markiewicz, and A. Bansil, Phys. Rev. B **67**, 014519 (2003).
[17] Tanmoy Das, R. S. Markiewicz, and A. Bansil, arXiv:0807.4257 (unpublished).
[18] V. Arpiainen, A. Bansil, and M. Lindroos, Phys. Rev. Lett. **103**, 067005 (2009).
[19] D. Manske, *Theory of Unconventional Superconductors: Cooper Pairing Mediated by Spin Excitations* (Springer, New York, 2004).
[20] Incidentally, the weak third band at higher binding energies in Figs. 1(e) and 1(f) is a lower lying band, which in the absence of self-energy corrections rises to higher energies.
[21] R. S. Markiewicz, S. Sahrakorpi, M. Lindroos, Hsin Lin, and A. Bansil, Phys. Rev. B **72**, 054519 (2005).
[22] k_z dispersion of the initial state is included through the TB parameter t_z=0.076 eV. Our bare-band bilayer splitting varies from around 120 meV at Γ to ~340 meV at $(\pi,0)$; the corresponding dressed values are ~60 and 150 meV.
[23] We use a rigid-band model to account for doping effects on the electronic spectrum. A more sophisticated treatment using Korringa-Kohn-Rostoker-coherent potential approximation or other approaches (see, e.g., Refs. 24–27) is not undertaken.
[24] A. Bansil, Z. Naturforsch., A: Phys. Sci. **48**, 165 (1993).
[25] L. Schwartz and A. Bansil, Phys. Rev. B **10**, 3261 (1974).
[26] S. N. Khanna, A. K. Ibrahim, S. W. McKnight, and A. Bansil, Solid State Commun. **55**, 223 (1985).
[27] H. Lin, S. Sahrakorpi, R. S. Markiewicz, and A. Bansil, Phys. Rev. Lett. **96**, 097001 (2006).
[28] A positive Σ' shifts bands closer to the Fermi level, while a negative value shifts bands away from the Fermi level.
[29] The antibonding band has an additional splitting associated with multiple poles of the Green's function at Γ [the line $\omega-\xi_{\Gamma}^{AB}$ coincides more than once with $\Sigma'(\omega)$, Fig. 2(a)].
[30] W. Meevasana, X. J. Zhou, S. Sahrakorpi, W. S. Lee, W. L. Yang, K. Tanaka, N. Mannella, T. Yoshida, D. H. Lu, Y. L. Chen, R. H. He, Hsin Lin, S. Komiya, Y. Ando, F. Zhou, W. X. Ti, J. W. Xiong, Z. X. Zhao, T. Sasagawa, T. Kakeshita, K. Fujita, S. Uchida, H. Eisaki, A. Fujimori, Z. Hussain, R. S. Markiewicz, A. Bansil, N. Nagaosa, J. Zaanen, T. P. Devereaux, and Z.-X. Shen, Phys. Rev. B **75**, 174506 (2007).
[31] The tails are typically produced at band bottoms due to the incoherent spectral weight introduced by the self-energy.
[32] We take the dimpling of the CuO_2 planes into account by using two different bilayer distances; d_1=2.9 Å for O and d_2=3.2 Å for Cu (Ref. 33).
[33] P. A. Miles, S. J. Kennedy, G. J. McIntyre, G. D. Gu, G. J. Russell, and N. Koshizuka, Physica C **294**, 275 (1998).
[34] D. L. Feng, C. Kim, H. Eisaki, D. H. Lu, A. Damascelli, K. M. Shen, F. Ronning, N. P. Armitage, N. Kaneko, M. Greven, J.-i. Shimoyama, K. Kishio, R. Yoshizaki, G. D. Gu, and Z.-X. Shen, Phys. Rev. B **65**, 220501(R) (2002).
[35] Value of the inner potential was obtained from an LDA slab calculation.
[36] It will be interesting to consider interplay between self-energy and matrix element effects along the lines of this study in other momentum-resolved spectroscopies (Refs. 37–40).
[37] Y. Tanaka, Y. Sakurai, A. T. Stewart, N. Shiotani, P. E. Mijnarends, S. Kaprzyk, and A. Bansil, Phys. Rev. B **63**, 045120 (2001).
[38] S. Huotari, K. Hämäläinen, S. Manninen, S. Kaprzyk, A. Bansil, W. Caliebe, T. Buslaps, V. Honkimäki, and P. Suortti, Phys. Rev. B **62**, 7956 (2000).
[39] L. C. Smedskjaer, A. Bansil, U. Welp, Y. Fangp, and K. G. Bailey, J. Phys. Chem. Solids **52**, 1541 (1991).
[40] R. S. Markiewicz and A. Bansil, Phys. Rev. Lett. **96**, 107005 (2006).
[41] C. Kusko, R. S. Markiewicz, M. Lindroos, and A. Bansil, Phys. Rev. B **66**, 140513(R) (2002). Within our model the pseudogap arises as the leading divergent susceptibility fluctuation mode.